

# Entanglement-assisted multiple-access channels: capacity regions and protocol designs

Haowei Shi,<sup>1</sup> Min-Hsiu Hsieh,<sup>2</sup> Saikat Guha,<sup>1</sup> Zheshen Zhang,<sup>3,1</sup> and Quntao Zhuang<sup>4,1,\*</sup>

<sup>1</sup>*James C. Wyant College of Optical Sciences, University of Arizona, Tucson, Arizona 85721, USA*

<sup>2</sup>*Hon Hai Research Institute, Taipei, Taiwan*

<sup>3</sup>*Department of Materials Science and Engineering,  
University of Arizona, Tucson, Arizona 85721, USA*

<sup>4</sup>*Department of Electrical and Computer Engineering,  
University of Arizona, Tucson, Arizona 85721, USA*

We solve the entanglement-assisted (EA) classical capacity region of quantum multiple-access channels with an arbitrary number of senders. As an example, we consider the bosonic thermal-loss multiple-access channel and solve the one-shot capacity region enabled by an entanglement source composed of sender-receiver pairwise two-mode squeezed vacuum states. The EA capacity region is strictly larger than the capacity region without entanglement-assistance, therefore also larger than the Yen-Shapiro rate-region of Gaussian encoding or coherent-state encoding. When the senders have transmitters of equal low brightness, we also numerically find that the two-mode squeezed vacuum source is optimal at a corner rate point. With two-mode squeezed vacuum states as the source and phase modulation as the encoding, we also design practical receiver protocols to realize the entanglement advantages. Four practical receiver designs, based on optical parametric amplifiers, are given and analyzed. In the parameter region of a large noise background, the receivers can enable a simultaneous rate advantage of 82.0% for each sender. Due to teleportation and superdense coding, our results for EA classical communication can be directly extended to EA quantum communication at half of the rate. Our work provides a unique and practical network communication scenario where entanglement can be beneficial.

## I. INTRODUCTION

Communication channels model physical media for information transmission. In the case of a single-sender single-receiver channel, the Shannon capacity theorem [1, 2] concludes that a channel is essentially characterized by a single quantity—the channel capacity. As physical media obey quantum physics, the channel model eventually needs to incorporate quantum effects during the transmission, which has re-shaped our understanding of communication. To begin with, the Shannon capacity has been generalized to the Holevo-Schumacher-Westmoreland (HSW) classical capacity [3–5]. Quantum effects such as entanglement have also enabled non-classical phenomena in communication, such as superadditivity [6–11] and capacity-boost from entanglement-assistance (EA) [12–21]. Moreover, reliable transmission of quantum information is possible, established by the Lloyd-Shor-Devetak quantum capacity theorem [22–24]. Combining different types of information transmission, Refs. 25 and 26 provide a capacity formula for the simultaneous trade-off of classical information (bits), quantum information (qubits) and quantum entanglement (ebits).

Despite their exact evaluation being prevented from the superadditivity dilemma, capacities of single-sender single-receiver quantum channels are well-understood. In particular, the benefits of entanglement in boosting the classical communication rates have been known since the pioneering theory works [12–15, 17] and recently experimentally demonstrated [27] in a thermal-

loss bosonic communication channel. The two-mode-squeezed-vacuum (TMSV) state is utilized as the entanglement source and functional quantum receivers are demonstrated, thanks to the practical protocol design in Ref. [28]. Further development of receiver designs [29] and the application to covert communication [30] have also been considered.

However, supported by the Internet, real-life communication scenarios, such as online lectures and online conferences, often involve multiple senders and/or receivers. As a common paradigm being studied in the literature, the multiple-access channel (MAC), concerns multiple senders and a single receiver. In this case, communication over the channel is no longer characterized by a single rate, but a trade-off capacity region of multiple communication rates between each sender and the single receiver. With the development of a quantum network [31–35], quantum effects have also become relevant in such a communication scenario. In this regard, the classical capacity region of a quantum MAC was solved by Winter [36], while the entanglement-assisted (EA) [37] classical communication capacity region of the special case of a two-sender MAC was solved in Ref. [17]. Although superadditivity in the capacity region has also been found in the MAC case [38, 39], it is unclear how much advantage entanglement can provide in this scenario.

In this work, we present a thorough study of EA classical communication over a quantum MAC with an arbitrary number of senders. On the fundamental information-theoretic side, we prove the general EA classical capacity theorem for an  $s$ -sender ( $s \geq 2$ ) MAC, which was conjectured in Ref. [17] and yet not proven for

\* zhuangquntao@email.arizona.edu

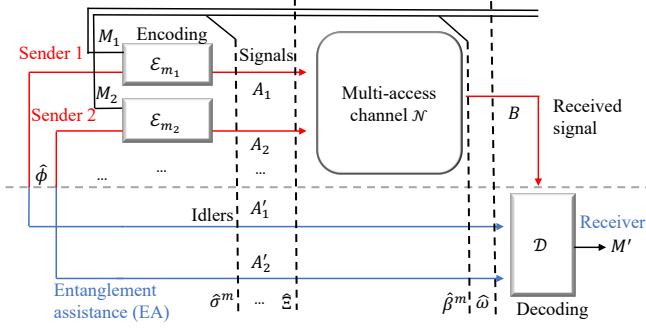


Figure 1. Schematic of a general EA-MAC communication protocol. The EA sources  $\phi$  of the  $s$  senders are in a product state of Eq. (1). The  $s$  senders apply independent encoding modeled by completely positive and trace-preserving operations, i.e., sender  $k$  applies  $\mathcal{E}_{m_k}$  on the signal state given the message  $m_k$ . Denoting the entire message as  $m = m_1 \cdots m_s$ , the encoded signal-idler is then in a state  $\hat{\sigma}^m$ . The senders' encoded quantum systems  $A = A_1 \cdots A_s$  are sent through the MAC  $\mathcal{N}$ , leading to the output system  $B$ . The receiver applies the quantum operation  $\mathcal{D}$  to decode the information from the joint state  $\hat{\beta}^m$  of the output system  $B$  and the pre-shared reference systems  $A' = A'_1 \cdots A'_s$ . We define  $M_k$  as the codeword space of each message  $m_k$ ,  $M$  as the overall codeword space of message  $m$ , and  $M'$  as the decoded codeword space. To facilitate the analysis, we denote the overall state  $\hat{\Xi}$  (Eq. (2)) over systems  $MAA'$  right before the channel and the overall state  $\hat{\omega}$  (Eq. (3)) over systems  $MBA'$  right before the decoding.

the past decade. Next, we give an explicit example of a bosonic thermal-loss MAC and evaluate its rate-region with the common TMSV entanglement source. We find great EA advantages over the case without EA, which has been studied by Ref [40]; Moreover, when the senders have equal low brightness, we numerically find that the TMSV source is optimal at a corner rate point, as the TMSV rate-region touches the EA outer bound. Finally, on the application side, we propose practical protocols to realize the EA advantage in a bosonic thermal-loss MAC, and provide multiple different transceiver designs. Due to teleportation [41] and superdense coding [12], our results for EA classical communication can be directly extended to EA quantum communication at half of the rate. As the bosonic thermal-loss MAC models various real-world communication networks, our EA communication scenario is widely applicable to radio-frequency (RF) communication, deep-space communication [42], and wireless communication scenario [43].

## II. MULTIPLE-ACCESS CHANNELS

In a MAC, multiple senders individually communicate with a single receiver. As depicted in Fig. 1, consider a MAC with  $s$  senders, each sending a message  $m_k$  ( $1 \leq k \leq s$ ) sampled from a codeword space  $M_k$ , therefore the overall message  $m = m_1 \cdots m_s$  is sampled from the

codeword space  $M = \otimes_{k=1}^s M_k$ . To send each message  $m_k$ , the  $k$ th sender performs a quantum operation  $\mathcal{E}_{m_k}$  to produce a signal quantum system  $A_k$ . Following Ref. [17], we introduce EA in the above communication scenario—namely the receiver has an reference system  $A'_k$  (idler) pre-shared as the EA with the  $k$ th sender, potentially delivered by a quantum network.

We consider the entanglement to be pairwise between each sender and the receiver such that the overall quantum state

$$\hat{\phi}_{AA'} = \otimes_{k=1}^s \hat{\phi}_{A_k A'_k} \quad (1)$$

is in a product form, where we have denoted  $A = A_1 \cdots A_s$  and  $A' = A'_1 \cdots A'_s$  as the overall systems. Therefore, each encoded signal-idler is in a state  $\hat{\sigma}_{A_k A'_k}^{m_k} = \mathcal{E}_{m_k} \otimes \mathcal{I}(\hat{\phi}_{A_k A'_k})$ , where  $\mathcal{I}$  is the identity channel modeling the ideal storage of the idler system. Denote the overall encoding operation as  $\mathcal{E}_m = \otimes_{k=1}^s \mathcal{E}_{m_k}$ , and the probability of sending each message as  $p_m = \prod_{k=1}^s p_{m_k}$ , the overall encoding can be described by the composite quantum state

$$\hat{\Xi}_{MAA'} = \sum_m p_m |m\rangle\langle m|_M \otimes \hat{\sigma}_{AA'}^m, \quad (2)$$

where  $\hat{\sigma}_{AA'}^m = \otimes_{k=1}^s \hat{\sigma}_{A_k A'_k}^{m_k} \equiv [\mathcal{E}_m \otimes \mathcal{I}](\hat{\phi}_{AA'})$  is the overall encoded state conditioned on message  $m$  and  $|m\rangle\langle m|_M$  is the classical register for message  $m$ .

After the encoding, all of the quantum systems from the  $s$  senders  $A$  are input to the MAC  $\mathcal{N}_{A \rightarrow B}$ , which outputs the quantum system  $B$  for the receiver to decode the messages jointly with the EA  $A'$ . The overall state after the channel is

$$\hat{\omega}_{MBA'} = \sum_m p_m |m\rangle\langle m|_M \otimes \hat{\beta}_{BA'}^m, \quad (3)$$

where  $\hat{\beta}_{BA'}^m = [\mathcal{N}_{A \rightarrow B} \otimes \mathcal{I}](\hat{\sigma}_{AA'}^m)$ . For convenience we also define a quantum state after the channel but without the encoding,

$$\hat{\rho}_{BA'} = [\mathcal{N}_{A \rightarrow B} \otimes \mathcal{I}](\hat{\phi}_{AA'}). \quad (4)$$

Note that in Eq. (4) we do not need the classical register  $M$  as no encoding is applied.

In this paper, we will focus on the bosonic thermal-loss MAC depicted in Fig. 2, which models an optical or microwave communication scenario. For example, it fits in the scenario where multiple mobile devices are communicating with the same signal station. Upon the input modes  $\hat{a}_{A_1} \cdots \hat{a}_{A_s}$  from the  $s$  senders, the MAC  $\mathcal{N}$  first combines the modes through a beam-splitter array to produce a mixture mode

$$\hat{a}_{A_{\text{mix}}} = \sum_{k=1}^s \sqrt{\eta_k} \hat{a}_{A_k}, \quad (5)$$

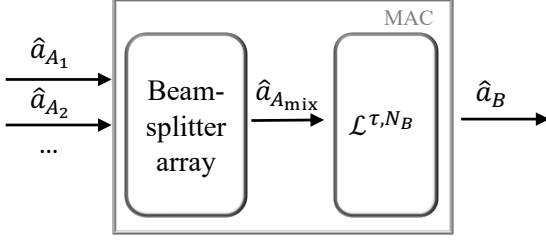


Figure 2. Schematic of the bosonic thermal-loss MAC. The beam-splitter array models a linear scattering medium. The thermal-loss channel models the noisy transmission.

while all other ports of the beam-splitter array are discarded, here the weights  $\{\eta_k\}$  are non-negative and normalized. Then the mixture mode goes through a bosonic thermal-loss channel  $\mathcal{L}^{\tau, N_B}$  described by the operator transform

$$\hat{a}_B = \sqrt{\tau}\hat{a}_{A_{\text{mix}}} + \sqrt{1-\tau}\hat{a}_E, \quad (6)$$

where  $\hat{a}_E$  denotes the environment mode in a thermal state with a mean photon number  $\langle a_E^\dagger a_E \rangle = N_B/(1-\tau)$ . This convention of fixing the mean photon number  $N_B$  of the thermal noise mixed into the output mode  $\hat{a}_B$  is widely used, e.g., in quantum illumination [44, 45].

In a bosonic MAC, as the Hilbert space of the quantum systems is infinite-dimensional—an arbitrary number of photons can occupy a single mode due to the bosonic nature of light. To model a realistic communication scenario, we will consider an energy constraint on the mean photon number (brightness) of the signals modes

$$\langle \hat{a}_{A_k}^\dagger \hat{a}_{A_k} \rangle = N_{S_k}, 1 \leq k \leq s, \quad (7)$$

which is commonly adopted in bosonic communication [28, 40, 46]. Note that in general the energy of different senders can be different.

The performance metric of the above communication scenario is described by a vector of rates  $(R_1, \dots, R_s)$ , where  $R_k$  is the reliable communication rate between the  $k$ th sender and the receiver. These rates in general have non-trivial trade-offs with each other. Formally, we define an  $(n, R_1, \dots, R_s, \epsilon)$  EA code by: each sender's encoding map  $\{\mathcal{E}_{m_k}\}, 1 \leq k \leq s$  on  $A$ , with each message  $m_k \in [2^{nR_k}]$ , and the decoding positive operator-valued measure (POVM)  $\{\hat{\Lambda}_{m_1 \dots m_s}\}$  on  $AA'$  such that

$$\text{Tr} \left\{ \hat{\Lambda}_{m_1 \dots m_s} [\mathcal{N}^{\otimes n} \circ (\otimes_{k=1}^s \mathcal{E}_{m_k}) \otimes \mathcal{I}_{A'}] \hat{\phi}_{AA'} \right\} \geq 1 - \epsilon. \quad (8)$$

We say that  $(R_1, \dots, R_s)$  is an achievable rate vector if for all  $\epsilon > 0, \delta > 0$  and sufficiently large  $n$ , there exists an  $(n, R_1 - \delta, \dots, R_s - \delta, \epsilon)$  EA code. The EA classical capacity region  $\mathcal{C}_E(\mathcal{N})$  is defined to be the closure of the set of all achievable rate vectors. In the case without EA,

the capacity region is well-established by the pioneering work of Winter [36] (see Appendix C for details).

To describe the rate region of the  $s$ -sender MAC, we will frequently divide the senders into two blocks, the block of interest indexed by a sequence  $J$  and the complementary block  $J^c$ . For example, when  $s = 2$ , we have four possible block divisions:  $\{J = 1, J^c = 2\}$ ,  $\{J = 2, J^c = 1\}$ ,  $\{J = 12, J^c = \emptyset\}$ , and a trivial case  $\{J = \emptyset, J^c = 12\}$ . Any  $s$ -fold quantity  $f$  can be written as a composition of the two blocks  $f = f[J]f[J^c]$ , defined by the mapping  $f[J] \rightarrow \otimes_{i \in J} f_i$ , e.g. codeword space  $M = M[J]M[J^c]$ , with  $M[J] = \otimes_{i \in J} M_i$ ,  $M[J^c] = \otimes_{i \in J^c} M_i$ ; similarly the message as  $m = m[J]m[J^c]$ .

Without EA, the capacity region of the above bosonic MAC has been considered in Ref. [40] for the two-user case. However, the generalization of the coherent-state rate region therein to the  $s$ -sender case is straightforward, leading to a rate region specified by the following  $2^s$  inequalities,

$$\sum_{i \in J} R_i \leq C_{\text{coh}}^J \equiv g \left( \sum_{i \in J} \tau \eta_i N_{S_i} + N_B \right) - g(N_B), \quad (9)$$

where  $g(x) = (x+1) \log_2(x+1) - x \log_2(x)$  and  $J$  can be chosen arbitrarily. Moreover, a squeezing-based encoding scheme is shown to be advantageous over the coherent-state encoding; however, regardless of the encoding, the rate region is always bounded by the following set of outer bounds

$$R_k \leq g(\tau N_{S_k} + N_B) - g(N_B), 1 \leq k \leq s, \quad (10)$$

which are derived by assuming a super receiver that can reverse the beamsplitter array in the bosonic thermal-loss MAC. A second outer bound can be obtained from energetic considerations, which leads to the same form of Ineq. (9) with  $J$  being all users. As these outer bounds represent the upper limit of all encodings without EA, an EA rate region outside the rate region specified by the above outer bounds will demonstrate a strict advantage enabled by entanglement.

### III. EA-MAC CAPACITY REGION

#### A. Capacity theorem

To present our EA-MAC capacity theorem for the scenario in Fig. 1, we introduce some entropic quantities. For a quantum system  $XYZ$  in a state  $\hat{\alpha}$ , we define the quantum mutual information between  $X$  and  $Y$  as

$$I(X : Y)_{\hat{\alpha}} = S(X)_{\hat{\alpha}} + S(Y)_{\hat{\alpha}} - S(XY)_{\hat{\alpha}}, \quad (11)$$

where  $S(X)_{\hat{\alpha}} = S(\hat{\alpha}_X) = -\text{tr}(\hat{\alpha}_X \log_2 \hat{\alpha}_X)$  is the von Neumann entropy. Similarly, the quantum conditional mutual information between  $X$  and  $Z$  conditioned on  $Y$

$$I(X; Z|Y)_{\hat{\alpha}} = S(XY)_{\hat{\alpha}} + S(YZ)_{\hat{\alpha}} - S(XYZ)_{\hat{\alpha}} - S(Y)_{\hat{\alpha}}. \quad (12)$$

With the entropic quantities in hand, we can present our main theorem below (see Appendix D for a proof).

**Theorem 1 EA-MAC capacity.** *The entanglement-assisted classical communication capacity region over an  $s$ -sender MAC  $\mathcal{N}$  is given by the regularized union*

$$\mathcal{C}_E(\mathcal{N}) = \overline{\bigcup_{n=1}^{\infty} \frac{1}{n} \mathcal{C}_E^{(1)}(\mathcal{N}^{\otimes n})} \quad (13)$$

where the “one-shot” region  $\mathcal{C}_E^{(1)}(\mathcal{N})$  is the union of “one-shot, one-encoding” regions

$$\mathcal{C}_E^{(1)}(\mathcal{N}) = \bigcup_{\hat{\phi}} \tilde{\mathcal{C}}_E(\mathcal{N}, \hat{\phi}). \quad (14)$$

The “one-shot, one-encoding” rate region  $\tilde{\mathcal{C}}_E(\mathcal{N}, \hat{\phi})$  for the  $2s$ -partite pure product state  $\hat{\phi}_{AA'} = \bigotimes_{k=1}^s \hat{\phi}_{A_k A'_k}$  over  $AA'$ , is the set of rates  $(R_1, \dots, R_s)$  satisfying the following  $2^s$  inequalities

$$\sum_{k \in J} R_k \leq I(A'[J]; B|A'[J^c])_{\hat{\rho}}, \forall J, \quad (15)$$

where the conditional quantum mutual information is evaluated over the output state  $\hat{\rho}_{BA'} = \mathcal{N}_{A \rightarrow B} \hat{\phi}_{AA'}$ .

Before proceeding to further bounds, we make three remarks about Theorem 1: First, the capacity region is convex due to time-sharing. Second, the capacity formula in Ref. [17] can be considered as a special case of our theorem; indeed, at the end of Ref. [17] our theorem is stated as a conjecture.

Similar to the case without EA, via reducing to the single-sender EA classical capacity, one can obtain outer bounds for the EA-MAC classical capacity region (See Appendix A for a proof). Explicitly, we have

$$R_k \leq C_E(N_{S_k}; \mathcal{L}^{\tau, N_B}), 1 \leq k \leq s, \quad (16a)$$

$$\sum_{k=1}^s R_k \leq C_E\left(\sum_{k=1}^s \eta_k N_{S_k}; \mathcal{L}^{\tau, N_B}\right), \quad (16b)$$

where the explicit formula of the EA capacity  $C_E(N_S; \mathcal{L}^{\tau, N_B})$  over a bosonic thermal-loss channel  $\mathcal{L}^{\tau, N_B}$ , with the energy constraint  $N_S$ , can be found in Eq. (A2) of Appendix A.

## B. Two-mode squeezed vacuum rate region

To obtain an explicit example of bosonic EA-MAC capacity region, we consider the entanglement source in Eq. (1) as a product of TMSV pairs, each with the wavefunction

$$\hat{\phi}_{A_k A'_k}^{\text{TMSV}} = \sum_{n_k=0}^{\infty} \sqrt{\frac{N_{S_k}^{n_k}}{(N_{S_k} + 1)^{n_k+1}}} |n_k\rangle_{A_k} |n_k\rangle_{A'_k}, \quad (17)$$

for  $1 \leq k \leq s$ , where  $|n\rangle$  is the number state defined by  $\hat{a}^\dagger \hat{a} |n\rangle = n |n\rangle$ . In Ref. [28], it has been shown that the TMSV state is optimal for single-sender single-receiver EA classical communication, therefore we expect the TMSV source to be good in the MAC case. Although, due to the complexity from the plurality of the senders, the exact union over the states in Eq. (14) for the EA-MAC classical capacity region is challenging to solve.

We evaluate the “one-shot, one-encoding” rate region  $\tilde{\mathcal{C}}_E(\mathcal{N}, \hat{\phi}^{\text{TMSV}})$  in Ineqs. (15) for the TMSV source in Eq. (17). Although the evaluation of each Ineq. (15) is efficient thanks to the Gaussian nature of the state, the number of such inequalities  $2^s$  is exponential and therefore resource-consuming in practice. To showcase the capacity region, we choose  $s = 2, 3$ , which enable direct visualization as the rate region is two or three dimensional. In comparison, we also compare with the classical coherent-state rate region in Ineq. (9) and the classical outer bound, specified by Ineq. (10) jointly and Ineq. (9) with  $J$  being all senders. Moreover, we can also compare  $\tilde{\mathcal{C}}_E(\mathcal{N}, \hat{\phi}^{\text{TMSV}})$  with the EA outer bound in Ineqs. (16).

Three representative setups of parameters are chosen

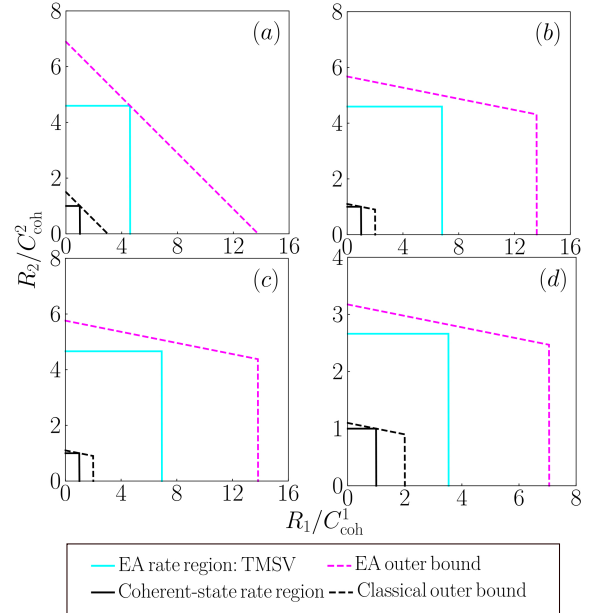


Figure 3. The symmetric two-sender rate region, normalized by the coherent-state bound  $C_{\text{coh}}^1, C_{\text{coh}}^2$  defined in Ineq. (9), evaluated at the scenario of (a) microwave domain,  $\tau = 0.01, N_B = 20, N_{S_1} = N_{S_2} = 0.01, \eta_1 = 1/3, \eta_2 = 2/3$ . (b) microwave domain,  $\tau = 0.01, N_B = 20, \eta_1 = \eta_2 = 1/2, N_{S_1} = 0.001, N_{S_2} = 0.01$ . (c) a noisy channel,  $\tau = 10^{-3}, N_B = 10^4, \eta_1 = \eta_2 = 1/2, N_{S_1} = 0.001, N_{S_2} = 0.01$ . (d) long wavelength infrared domain  $\eta_1 = \eta_2 = 1/2, \tau = 0.001, N_B = 0.1, N_{S_1} = 0.001, N_{S_2} = 0.01$ . The EA rate region in Ineq. (15) (cyan solid), evaluated on TMSV states, is bounded by the EA outer bound (magenta dashed) in Ineqs. (16); while the coherent-state rate region (black solid) given by Ineq. (9) is bounded by the classical outer bound (black dashed).



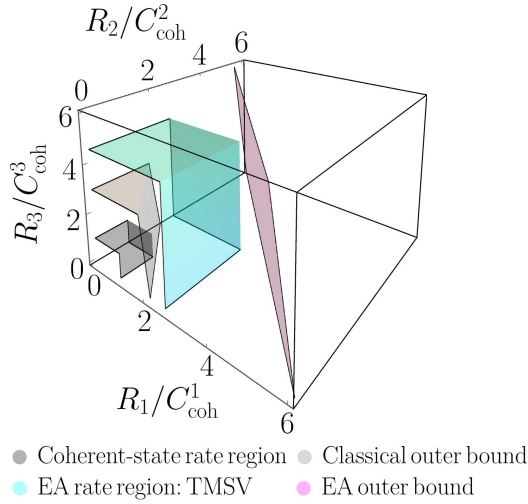


Figure 4. The asymmetric three-sender EA rate region normalized by the coherent state bound  $C_{\text{coh}}^1$ ,  $C_{\text{coh}}^2$  and  $C_{\text{coh}}^3$  defined in Ineq. (9), evaluated at the scenario of microwave domain  $N_{S_1} = N_{S_2} = 0.1$ ,  $N_{S_3} = 0.01$ ,  $\tau = 0.01$ ,  $N_B = 20$ ,  $\eta_1 = \eta_2 = \eta_3 = 1/3$ . The EA rate region in Ineq. (15) (cyan), evaluated on TMSV states, is bounded by the EA outer bound (magenta) in Ineqs. (16); while the coherent-state rate region (black) given by Ineq. (9) is bounded by the classical outer bound (light gray).

as examples. To begin with, we consider an intermediate channel noise  $N_B = 20$ , identical to the case of microwave quantum illumination [44, 47]; Furthermore, a noisy channel with sufficiently large noise  $N_B = 10^4$  is noteworthy as it provides a saturated EA advantage [28]; Finally, the long wavelength infrared domain with relatively small noise  $N_B = 0.1$  is a relatively uncharted territory for EA communication, nevertheless also relevant for practical application.

We begin with a two-sender case ( $s = 2$ ). As shown in Fig. 3, in all the parameter settings being considered, we can see strict advantages of the EA capacity region (cyan solid) over the classical outer bound (black dashed), which is higher than the coherent-state rate region (black solid). We find that the advantage is larger when the noise  $N_B$  is larger, comparing subplot (c) and (d). In particular, this advantage also holds when  $N_S \ll N_B \ll 1$ , which can happen in the long wavelength infrared domain, as shown in subplot (d).

Comparing with the EA outer bound (magenta dashed), we see that in Fig. 3(a) the TMSV rate region (cyan solid) touches the EA outer bound (magenta dashed) at a corner point when  $R_2/C_{\text{coh}}^2 = R_1/C_{\text{coh}}^1$  to the leading order. The gap is of the order of  $10^{-5}$  relatively; therefore, at this point, the TMSV source is in fact optimal for the thermal-loss MAC being considered, for this symmetric case where the parameters  $N_{S_k} \ll 1$  are identical among the senders. Note this holds although the transmissivities of the senders  $\eta_k$  are not equal. In other cases, when  $N_{S_1} \neq N_{S_2}$ , regardless of the values

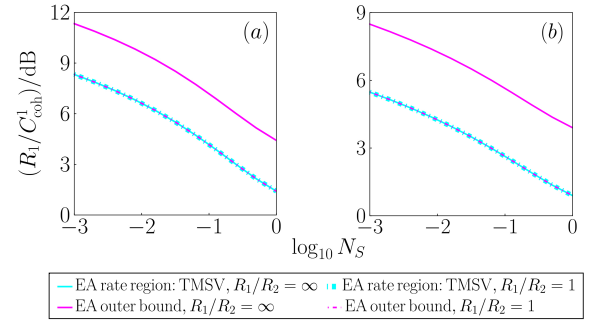


Figure 5. The dependence on source brightness  $N_{S_1} = N_{S_2} = N_S$  of the EA advantage of the EA rate regions for two-sender MAC communication under the scenario of (a) microwave domain  $\eta = 1/2$ ,  $\tau = 0.01$ ,  $N_B = 20$ ; (b) long wavelength infrared domain  $\eta_1 = \eta_2 = 1/2$ ,  $\tau = 0.001$ ,  $N_B = 0.1$ . We plot  $R_1$  for sender 1 under different  $R_1/R_2$  conditions. Note that  $R_1/R_2 = 0, \infty$  are equivalent up to a swap due to the symmetry between the two senders; and for given  $R_1/R_2$ ,  $R_2/C_{\text{coh}}^2 = R_1/C_{\text{coh}}^1$ . We also compare the EA rate region of TMSV (cyan) with the EA outer bound (magenta).

of  $\eta_k$  being equal, a strict gap between the TMSV rate region and the EA outer bound exists for all rates. This does not conclude that the TMSV is inferior, though, as the outer bound is likely to be loose.

Now we consider a three-sender asymmetric case ( $s = 3$ ), with unequal source brightness  $N_{S_1} = N_{S_2} \neq N_{S_3}$ . In Fig. 4, a gap emerges between the TMSV rate region (the region below the cyan surface) and the outer bound (the magenta surface), as we expected. An appreciable EA advantage remains several times beyond the coherent state rate region (dark gray surface) and the classical outer bound (light gray surface).

Now we further consider the scaling of the EA advantage observed above. As shown in Fig. 5, the advantage of the EA capacity (magenta) relative to the case without EA also diverges with  $\log(N_S)$ , when the signal brightness  $N_S$  is small, while the noise  $N_B$  is much larger than the signal brightness  $N_S$ . Note that this advantage also holds for the case when  $N_S \ll N_B < 1$ , as shown in Fig. 5(b). This logarithmic diverging EA advantage in MAC case is similar to the case of single-sender single-receiver studied in Ref. [28]. Indeed, at the limit  $\tau \rightarrow 0$ ,  $N_S \ll 1$ , the relative ratio of the outer bound over the coherent-state rate

$$\frac{C_E(N_{S_k}; \mathcal{L}^{\tau, N_B})}{C_{\text{coh}}^k} \simeq \frac{\log(1/N_{S_k})}{\eta_k(1 + N_B) \log(1 + 1/N_B)}, \quad (18)$$

is also logarithmic in  $1/N_{S_k}$  when  $N_B$  is small.

#### IV. PROTOCOL DESIGN FOR BOSONIC EA-MAC

In this section, we design a practical protocol to realize EA classical communication over the bosonic thermal-

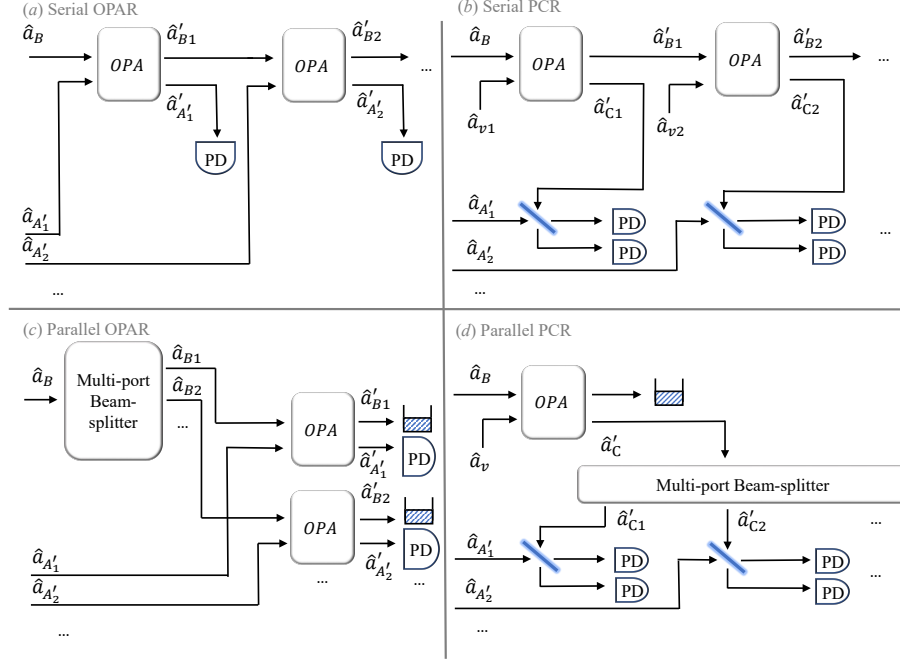


Figure 6. Schematic of four receiver designs: (a) serial optical-parametric-amplifier receiver (sOPAR) (b) serial phase-conjugate receiver (sPCR) (c) parallel optical-parametric-amplifier receiver (pOPAR) (d) parallel phase-conjugate receiver (pPCR).

loss MAC. The protocol consists of phase-modulation encoding on the TMSV entanglement source and structured receiver designs.

### A. Encoding and receiver designs

Similar to the single-sender single-receiver case, to encode a bit of information  $\{m_k = 0, 1, 1 \leq k \leq s\}$ , each sender performs a phase modulation on the signal part of the TMSV pairs via a unitary

$$\mathcal{E}_{m_k} = e^{im_k \pi \hat{a}_{A_k}^\dagger \hat{a}_{A_k}}, 1 \leq k \leq s, \quad (19)$$

to produce the quantum system  $\{A_k, 1 \leq k \leq s\}$  input to the MAC, while the idler part of the TMSV pairs  $\{A'_k, 1 \leq k \leq s\}$  is pre-shared to the receiver side for EA. Here we have considered the binary phase shift keying (BPSK): the  $k$ th sender sends the bit message 0, 1 by the same probability  $p_0 = p_1 = 1/2$ . In general, one can also consider higher-order phase keying, however, the rate performance will be similar. To enable efficient decoding, we consider  $N_R$  repetition of such encoding—each message is repeatedly encoded on  $N_R$  signal modes of a single sender.

The decoding process takes the output of the MAC  $\hat{a}_B$  and the EA idlers  $\{\hat{a}_{A'_k}, 1 \leq k \leq s\}$  to decode the information  $\{m_k, 1 \leq k \leq s\}$  of all the senders. Below we propose four receiver designs for the decoding. The basic element in the receiver design is the optical parametric amplifier (OPA), which upon input modes  $\hat{a}_R$  and  $\hat{a}_I$ ,

produces two modes

$$\begin{aligned} \hat{a}'_R &= \sqrt{G}\hat{a}_R + \sqrt{G-1}\hat{a}_I^\dagger, \\ \hat{a}'_I &= \sqrt{G}\hat{a}_I + \sqrt{G-1}\hat{a}_R^\dagger, \end{aligned} \quad (20)$$

where  $G$  is the gain of the OPA. An OPA transforms the phase-sensitive correlation between the input mode-pair into the photon number difference  $\langle \hat{a}_I'^\dagger \hat{a}_I' \rangle \propto \sqrt{G(G-1)} 2\text{Re} \langle \hat{a}_I \hat{a}_R \rangle$ , which is widely utilized to design receivers in EA applications, such as quantum illumination [47] and the bipartite EA classical communication [28]. Moreover, one can use an OPA as a phase-conjugator to design a phase-conjugate receiver (PCR), as explained in Ref. [28].

To decode all  $s$  messages, one can apply two different strategies, either decode them in a serial manner or in parallel. One can also base the receiver design on the direct OPA or on the phase-conjugation mechanism. These choices lead to four receiver designs—serial OPAR, serial PCR, parallel OPAR and parallel PCR—as we summarize below (see details in Appendix B).

In the serially connected scheme, on the  $k$ th round, the signal output  $\hat{a}'_{B_{k-1}}$  from the  $(k-1)$ th round and the idler  $\hat{a}_{A_k}$  are input to an OPA. The idler mode output from the OPA is detected, by direct detection in serial OPAR or an interferometric detection in serial PCR, to decode the message from the  $k$ th sender. Meanwhile, the signal mode output from the OPA is further utilized in the next round. Note that after the  $k$ th round, the cross correlation between the signal mode with the other idler

modes are almost intact; therefore, performing an OPA on the signal and another idler  $\hat{a}_{A'_k}$ , one can decode the message from the  $k$ 'th sender. Iterating this procedure on the remaining mode consecutively, one obtains a serial architecture for the receiver, as shown in Fig. 6 (a)(b) for the serial OPA-receiver (OPAR) and serial PCR.

We can also adopt a parallel design for the receivers. As the thermal-loss channel in the MAC adds excess noise into the output, we expect that in the noisy case, splitting the returned signal into  $s$  copies, each for the decoding of the message of a single sender, will still provide similar signal-to-noise ratios, when compared to the case without the splitting. In this way, each portion of the returned signal can be utilized in parallel, in each individual OPA component in the parallel OPAR or in each phase-conjugation detection in the parallel PCR, to decode each message. As shown in Fig. 6 (c)(d), we can design parallel-OPAR and parallel-PCR schemes.

## B. Receiver rate region evaluations

As the receivers are chosen, now the rate region is entirely obtained from the classical formula [2] com-

$$I(M[J]; B_R | M[J^c]) = \sum_{m[J^c]} p_{m[J^c]} \left\{ H \left[ \left\{ \sum_{m[J]} p_{m[J]} P(\mathbf{n}|m) \right\}_{\mathbf{n}} \right] - \sum_{m[J]} p_{m[J]} H[\{P(\mathbf{n}|m)\}_{\mathbf{n}}] \right\}, \quad (21)$$

where  $H[\{P(\mathbf{n})\}_{\mathbf{n}}] = -\sum_{\mathbf{n}} P(\mathbf{n}) \log P(\mathbf{n})$  is the Shannon entropy of the distribution  $P$ . Different from the quantity  $I(M[J]; B | M[J^c])$ , here Eq. (21) is the formula of the optimum information rate for a specific measurement strategy given by one of the four receiver designs. Unfortunately, the decoding protocol is not separable per sender, which actually involves the joint decoding over all the outputs of photon detectors and all the letters of the whole codeword.

We evaluate the (soft-decoding) rate regions of our four receivers in the case of phase-modulated TMSVs, as shown in Fig. 7. While the performances of OPAR are evaluated exactly, the performances of PCR are evaluated with a Gaussian approximation on the photon statistics, which is precise when the number of repetition modes  $N_R$  is large (see Appendix B for details). We compare the receiver rate regions with the classical coherent-state rate region in Ineq. (9) (black solid) and the classical outer bound in Ineq. (10) jointly and Ineq. (9) (black dashed) with  $J$  being all senders. We see that the performance of both OPAR and PCR can beat the classical coherent state rate region and the classical outer bound.

In Fig. 7, the performance of the OPAR (blue solid and

red solid) is inferior to the PCR (purple solid and orange solid), a gap between which is significant in Fig. 7(a). This is because the PCR has a better signal-to-noise ratio to the next order in  $N_S$  compared with OPA, as found in the single-sender case in Ref. [28] and confirmed in Fig. 8 here. As the brightness  $N_S$  decreases in Fig. 7(b), the gap between the PCR and OPAR almost diminishes. In Fig. 8, we see the rates of OPAR (blue and red) are lower than PCR (purple and orange), with a gap expanding as the brightness  $N_S$  grows. We also find that the rate advantage of both the OPAR and PCR saturates to 3dB as the brightness  $N_S$  decreases, consistent with the signal-to-noise ratio advantage in quantum illumination [44, 45]. This is because when the noise is large, the information rate is proportional to the signal-to-noise ratio. Note that when the channel noise  $N_B$  decreases, i.e. deviated from the quantum illumination scenario, the theoretical EA advantage evaluated by TMSV remains substantial. However, the practical advantage allowed by our receivers diminishes as  $N_B$  falls below 1. For  $N_B = 0.1$  (and smaller), there is no advantage for the proposed receivers, as shown in Fig. 8(b). This leaves an open question that a feasible receiver that provides EA advantage in the low-noise scenario is hitherto elusive.

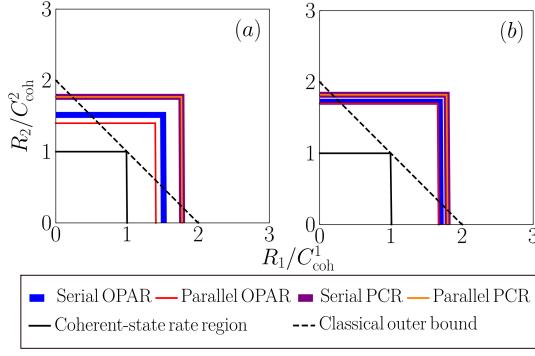


Figure 7. The two-sender rate region of our four receivers, normalized by the coherent state bound  $C_{\text{coh}}^1$ ,  $C_{\text{coh}}^2$  defined in Ineq. (9): (a) microwave domain  $N_{S1} = N_{S2} = 0.01$ ,  $\tau = 0.01$ ,  $N_B = 20$ ,  $\eta_1 = \eta_2 = 1/2$ ,  $N_R = 2 \times 10^4$ ; (b) a noisy channel with  $N_{S1} = N_{S2} = 10^{-3}$ ,  $\tau = 10^{-3}$ ,  $N_B = 10^4$ ,  $\eta = 1/2$ ,  $N_R = 10^7$ . To distinguish between the overlapping lines, we plot the serial receivers in thicker lines by contrast with the parallel receivers plotted narrowed. The gains of OPAR are given in the main text, and the gains of PCR are  $G = 2$  for  $N_B = 20$  and  $G = 1 + 10^{-3}$  for  $N_B = 10^4$ . We also compare the receiver rate region with the coherent-state rate (black solid) region and the classical outer bound (black dashed).

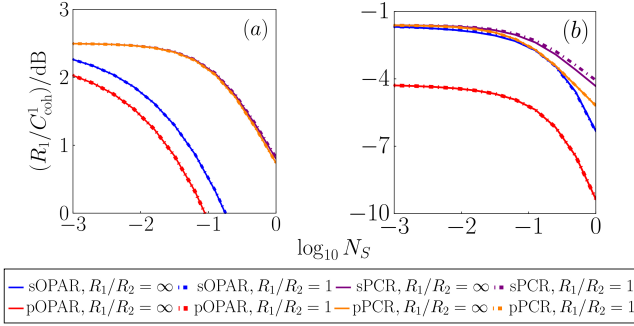


Figure 8. The dependence on source brightness  $N_{S1} = N_{S2} = N_S$  of the EA advantage of the four receivers for two-sender MAC communication under the scenario of (a) microwave domain  $\eta = 1/2$ ,  $\tau = 0.01$ ,  $N_B = 20$ ; (b) long wavelength infrared domain  $\eta_1 = \eta_2 = 1/2$ ,  $\tau = 0.001$ ,  $N_B = 0.1$ . In the legend s, p refer to ‘serial’ and ‘parallel’ respectively. The number of modes  $N_R$  is fixed such that the signal-to-noise ratio  $N_R \tau N_S / N_B = 0.1$  for sender  $i = 1, 2$ . We plot  $R_1$  for sender 1 under different  $R_1/R_2$  conditions. Note that  $R_1/R_2 = 0, \infty$  are equivalent up to a swap due to the symmetry between the two senders; and for given  $R_1/R_2$ ,  $R_2/C_{\text{coh}}^2 = R_1/C_{\text{coh}}^1$ .

## V. DISCUSSION

In this paper, we have solved the capacity region of entanglement-assisted classical communication over a quantum multiple-access channel with an arbitrary number of senders. We also provide explicit encoding and decoding strategies that provide a practical route towards achieving quantum advantages in such network communication scenarios. Due to teleportation [41] and superdense coding [12], the rate region of EA quantum communication is precisely half of the EA classical communication region; therefore, all of our results can straightforwardly extended to the case of quantum communication. The explicit protocols can also be used for EA quantum communication via further combining with a teleportation protocol.

Many future directions can be explored. For example, multi-partite entanglement may be considered instead of the product form of Eq. (1) to assist the communication scenario, when the senders can collaborate. Another open question is whether one can have superadditivity phenomena in our entanglement-assisted capacity region of multiple-access channels.

## ACKNOWLEDGMENTS

This project is supported by the Defense Advanced Research Projects Agency (DARPA) under Young Faculty Award (YFA) Grant No. N660012014029, National Science Foundation (NSF) Engineering Research Center for Quantum Networks Grant No. 1941583 and “Superconducting Quantum Materials and Systems” U.S. DOE National Quantum Information Science Research Center, DE-FOA-0002253. Q.Z. also acknowledges Craig M. Berge Dean’s Faculty Fellowship of University of Arizona. Z.Z. is supported in part by NSF Grant No. ECCS-1920742 and No. CCF-1907918. Q.Z. thanks Moe Z. Win for helpful discussions.

[1] C. Shannon, A mathematical theory of communication bell, Syst. Tech. J. **27**, 379 (1948).  
[2] T. M. Cover, *Elements of information theory* (John Wiley & Sons, 1999).  
[3] P. Hausladen, R. Jozsa, B. Schumacher, M. Westmoreland, and W. K. Wootters, Classical information capacity of a quantum channel, Phys. Rev. A **54**, 1869 (1996).  
[4] B. Schumacher and M. D. Westmoreland, Sending classical information via noisy quantum channels, Phys. Rev.

A **56**, 131 (1997).  
[5] A. S. Holevo, The capacity of the quantum channel with general signal states, IEEE Trans. Inf. Theory **44**, 269 (1998).  
[6] M. B. Hastings, Superadditivity of communication capacity using entangled inputs, Nat. Phys. **5**, 255 (2009).  
[7] G. Smith and J. Yard, Quantum communication with zero-capacity channels, Science **321**, 1812 (2008).  
[8] E. Y. Zhu, Q. Zhuang, and P. W. Shor, Superadditivity



- of the classical capacity with limited entanglement assistance, *Phys. Rev. Lett.* **119**, 040503 (2017).
- [9] E. Y. Zhu, Q. Zhuang, M.-H. Hsieh, and P. W. Shor, Superadditivity in trade-off capacities of quantum channels, *IEEE Trans. Inf. Theory* (2018).
  - [10] F. Leditzky, D. Leung, and G. Smith, Dephasing channel and superadditivity of coherent information, *Phys. Rev. Lett.* **121**, 160501 (2018).
  - [11] M. Fanizza, F. Kianvash, and V. Giovannetti, Quantum flags and new bounds on the quantum capacity of the depolarizing channel, *Phys. Rev. Lett.* **125**, 020503 (2020).
  - [12] C. H. Bennett and S. J. Wiesner, Communication via one-and two-particle operators on einstein-podolsky-rosen states, *Phys. Rev. Lett.* **69**, 2881 (1992).
  - [13] C. H. Bennett, P. W. Shor, J. A. Smolin, and A. V. Thapliyal, Entanglement-assisted classical capacity of noisy quantum channels, *Phys. Rev. Lett.* **83**, 3081 (1999).
  - [14] C. H. Bennett, P. W. Shor, J. A. Smolin, and A. V. Thapliyal, Entanglement-assisted capacity of a quantum channel and the reverse shannon theorem, *IEEE Trans. Inf. Theory* **48**, 2637 (2002).
  - [15] A. S. Holevo, On entanglement-assisted classical capacity, *J. Math. Phys.* **43**, 4326 (2002).
  - [16] P. W. Shor, The classical capacity achievable by a quantum channel assisted by limited entanglement, *arXiv quant-ph/0402129* (2004).
  - [17] M.-H. Hsieh, I. Devetak, and A. Winter, Entanglement-assisted capacity of quantum multiple-access channels, *IEEE Trans. Inf. Theory* **54**, 3078 (2008).
  - [18] Q. Zhuang, E. Y. Zhu, and P. W. Shor, Additive classical capacity of quantum channels assisted by noisy entanglement, *Phys. Rev. Lett.* **118**, 200503 (2017).
  - [19] M. M. Wilde and M.-H. Hsieh, The quantum dynamic capacity formula of a quantum channel, *Quantum Inf. Process.* **11**, 1431 (2012).
  - [20] M. M. Wilde, P. Hayden, and S. Guha, Information trade-offs for optical quantum communication, *Phys. Rev. Lett.* **108**, 140501 (2012).
  - [21] Q. Zhuang, Entanglement-assisted classical communication without a phase reference, *arXiv:2010.11974* (2020).
  - [22] S. Lloyd, Capacity of the noisy quantum channel, *Phys. Rev. A* **55**, 1613 (1997).
  - [23] P. W. Shor, The quantum channel capacity and coherent information, in *lecture notes, MSRI Workshop on Quantum Computation* (2002).
  - [24] I. Devetak, The private classical capacity and quantum capacity of a quantum channel, *IEEE Trans. Inf. Theory* **51**, 44 (2005).
  - [25] M. M. Wilde and M.-H. Hsieh, The quantum dynamic capacity formula of a quantum channel, *Quantum Inf. Process.* **11**, 1431 (2012).
  - [26] M. M. Wilde, P. Hayden, and S. Guha, Quantum trade-off coding for bosonic communication, *Phys. Rev. A* **86**, 062306 (2012).
  - [27] S. Hao, H. Shi, W. Li, Q. Zhuang, and Z. Zhang, Entanglement-assisted communication surpassing the ultimate classical capacity, *arXiv preprint arXiv:2101.07482* (2021).
  - [28] H. Shi, Z. Zhang, and Q. Zhuang, Practical route to entanglement-assisted communication over noisy bosonic channels, *Phys. Rev. Applied* **13**, 034029 (2020).
  - [29] S. Guha, Q. Zhuang, and B. A. Bash, Infinite-fold enhancement in communications capacity using pre-shared entanglement, in *2020 ISIT* (IEEE, 2020) pp. 1835–1839.
  - [30] C. N. Gagatsos, M. S. Bullock, and B. A. Bash, Covert capacity of bosonic channels, *IEEE J. Sel. Area Inf. Theory* **1**, 555 (2020).
  - [31] H. J. Kimble, The quantum internet, *Nature* **453**, 1023 (2008).
  - [32] J. Biamonte, M. Faccin, and M. De Domenico, Complex networks from classical to quantum, *Commun. Phys.* **2**, 53 (2019).
  - [33] S. Wehner, D. Elkouss, and R. Hanson, Quantum internet: A vision for the road ahead, *Science* **362** (2018).
  - [34] W. Kozłowski and S. Wehner, Towards large-scale quantum networks, in *Proceedings of the Sixth Annual ACM International Conference on Nanoscale Computing and Communication* (2019) pp. 1–7.
  - [35] B. Zhang and Q. Zhuang, Entanglement formation in continuous-variable random quantum networks, *arXiv:2005.12934*. To appear in *npj Quantum Inf.* (2020).
  - [36] A. Winter, The capacity of the quantum multiple-access channel, *IEEE Trans. Inf. Theory* **47**, 3059 (2001).
  - [37] We use ‘EA’ to denote both entanglement-assistance and entanglement-assisted.
  - [38] L. Czekaj and P. Horodecki, Purely quantum superadditivity of classical capacities of quantum multiple access channels, *Phys. Rev. Lett.* **102**, 110505 (2009).
  - [39] L. Czekaj, Subadditivity of the minimum output entropy and superactivation of the classical capacity of quantum multiple access channels, *Phys. Rev. A* **83**, 042304 (2011).
  - [40] B. J. Yen and J. H. Shapiro, Multiple-access bosonic communications, *Phys. Rev. A* **72**, 062312 (2005).
  - [41] C. H. Bennett, G. Brassard, C. Crépeau, R. Jozsa, A. Peres, and W. K. Wootters, Teleporting an unknown quantum state via dual classical and einstein-podolsky-rosen channels, *Phys. Rev. Lett.* **70**, 1895 (1993).
  - [42] K. Banaszek, L. Kunz, M. Jarzyna, and M. Jachura, Approaching the ultimate capacity limit in deep-space optical communication, *Proc. SPIE 10910, Free-Space Laser Communications XXXI*, 109100A (2019).
  - [43] M. Z. Win and R. A. Scholtz, Ultra-wide bandwidth time-hopping spread-spectrum impulse radio for wireless multiple-access communications, *IEEE Trans. Inf. Theory* **48**, 679 (2000).
  - [44] S.-H. Tan, B. I. Erkmen, V. Giovannetti, S. Guha, S. Lloyd, L. Maccone, S. Pirandola, and J. H. Shapiro, Quantum illumination with gaussian states, *Phys. Rev. Lett.* **101**, 253601 (2008).
  - [45] Q. Zhuang, Z. Zhang, and J. H. Shapiro, Optimum mixed-state discrimination for noisy entanglement-enhanced sensing, *Phys. Rev. Lett.* **118**, 040801 (2017).
  - [46] V. Giovannetti, R. Garcia-Patron, N. J. Cerf, and A. S. Holevo, Ultimate classical communication rates of quantum optical channels, *Nat. Photonics* **8**, 796 (2014).
  - [47] S. Guha and B. I. Erkmen, Gaussian-state quantum-illumination receivers for target detection, *Phys. Rev. A* **80**, 052310 (2009).

## Appendix A: Outer bounds for bosonic thermal-loss MAC

Now we provide the outer bound in Ineqs. (16) for the EA classical capacity region of the bosonic thermal-loss MAC. As we see in Fig. 2, the overall channel can be

written as a concatenation of two parts,  $\mathcal{N} = \mathcal{L}^{\tau, N_B} \circ \mathcal{E}_{\text{MAC}}$ , where  $\mathcal{E}_{\text{MAC}}$  represents the beamsplitter modeling the signal interference. From the bottleneck inequality, the overall communication rate is upper bounded by

$$\sum_{k=1}^s R_k \leq C_E \left( \sum_{k=1}^s \eta_k N_{S_k}; \mathcal{L}^{\tau, N_B} \right), \quad (\text{A1})$$

the single-sender single-receiver EA classical capacity of the thermal-loss channel  $\mathcal{L}^{\tau, N_B}$  with brightness  $\sum_{k=1}^s \eta_k N_{S_k}$ . This is because for the channel  $\mathcal{L}^{\tau, N_B}$ , only a single mode signal  $\hat{a}_{A_{\text{mix}}}$  in Eq. (5) with brightness  $\langle \hat{a}_{A_{\text{mix}}}^\dagger \hat{a}_{A_{\text{mix}}} \rangle = \sum_{k=1}^s \eta_k N_{S_k}$  goes through. Explicitly, the capacity

$$C_E(N_S; \mathcal{L}^{\tau, N_B}) = g(N_S) + g(N'_S) - g(A_+) - g(A_-), \quad (\text{A2})$$

with  $A_\pm = (D - 1 \pm (N'_S - N_S))/2$ ,  $N'_S = \tau N_S + N_B$  and  $D = \sqrt{(N_S + N'_S + 1)^2 - 4\tau N_S(N_S + 1)}$ . This proves Ineq. (16b).

As for the individual upper bounds for the senders in Ineq. (16a), we consider a theoretical super-receiver with access to all of the output ports of the beamsplitter part. The super-receiver performs the reverse of the beamsplitter transform, after which the communication reduces to the single-sender scenario of which the information rate is bounded by each single-sender single-receiver EA classical capacity. Explicitly, we have

$$R_k \leq C_E(N_{S_k}; \mathcal{L}^{\tau, N_B}), 1 \leq k \leq s, \quad (\text{A3})$$

which proves Ineq. (16a).

## Appendix B: Analyses of the receiver designs

To begin with, we briefly summarize the receiver problem to be solved in this section. Note that in this sec-

tion, we will write subscripts inside subscripts as normal texts so that the equations are not too small to be visible. In the phase encoding scheme, each sender applies a phase rotation on the signal mode  $\hat{a}_{A_k}$  of its TMSV source, which modules the signal-idler correlations by  $\langle \hat{a}_{A_k} \hat{a}_{A'_k} \rangle = C_{pk} \equiv \sqrt{N_{S_k}(N_{S_k} + 1)} e^{i\theta_k}$ . For binary encoding, each  $\theta_k$  has two possible values  $\theta_k^{(0)} = 0, \theta_k^{(1)} = \pi$ . The signal modes  $\hat{a}_{A_k}$  then goes through the thermal-loss MAC, which produces the received mode  $\hat{a}_B$  given by Eq. (5) and Eq. (6).

Below we assess the receivers in the two-sender scenario as an example. The  $s$ -sender case is solved in the same way. For convenience, let  $\eta_1 = \eta, \eta_2 = 1 - \eta$ . To ease the reading, we mark the modes after the OPAs with the superscript ' $r$ '.

### 1. Serial OPAR (Fig. 6a)

For the first OPA with a gain  $G_1$ ,

$$\begin{aligned} \hat{a}'_{B1} &= \sqrt{G_1} \hat{a}_B + \sqrt{G_1 - 1} \hat{a}_{A'_1}^\dagger, \\ \hat{a}'_{A'_1} &= \sqrt{G_1} \hat{a}_{A'_1} + \sqrt{G_1 - 1} \hat{a}_B^\dagger. \end{aligned} \quad (\text{B1})$$

We measure the photon counts of  $N_R$  independent and identical (i.i.d.) copies of  $\hat{a}'_{A'_1}$ .

For the second OPA with a gain  $G_2$ ,

$$\begin{aligned} \hat{a}'_{B2} &= \sqrt{G_2} \hat{a}'_{B1} + \sqrt{G_2 - 1} \hat{a}_{A'_2}^\dagger, \\ \hat{a}'_{A'_2} &= \sqrt{G_2} \hat{a}_{A'_2} + \sqrt{G_2 - 1} \hat{a}'_{B1}^\dagger. \end{aligned} \quad (\text{B2})$$

We measure the photon counts of  $N_R$  i.i.d. copies of  $\hat{a}'_{A'_2}$ .

We make decision on the  $N_R$  i.i.d photon counts of modes  $\hat{a}'_{A'_1}, \hat{a}'_{A'_2}$ . Indeed,  $\hat{a}'_{A'_1}, \hat{a}'_{A'_2}$  are in a zero-mean Gaussian state with the covariance matrix

$$V \equiv \left\langle \begin{pmatrix} \hat{a}'_{A'_1} \\ \hat{a}'_{A'_1}^\dagger \\ \hat{a}'_{A'_2} \\ \hat{a}'_{A'_2}^\dagger \end{pmatrix} \begin{pmatrix} \hat{a}'_{A'_1}^\dagger & \hat{a}'_{A'_1} & \hat{a}'_{A'_2}^\dagger & \hat{a}'_{A'_2} \end{pmatrix} \right\rangle = \begin{pmatrix} a+1 & 0 & c & 0 \\ 0 & a & 0 & c^* \\ c^* & 0 & s+1 & 0 \\ 0 & c & 0 & s \end{pmatrix}, \quad (\text{B3})$$

where the constants

$$\begin{aligned} a &= G_1 N_{S1} + 2\sqrt{(G_1 - 1) G_1 \tau \eta} \text{Re } C_{p1} + (G_1 - 1) [1 + N_B + N_S^*], \\ s &= G_2 N_{S2} + 2\sqrt{(G_2 - 1) G_2 G_1 \tau (1 - \eta)} \text{Re } C_{p2} \\ &\quad + (G_2 - 1) \left\{ (G_1 - 1) N_{S1} + G_1 [1 + N_B + N_S^*] + 2 \text{Re } \sqrt{(G_1 - 1) G_1 \tau \eta} C_{p1} \right\}, \\ c &= \sqrt{(G_2 - 1)} \left[ \sqrt{(G_1 - 1) G_1} (N_S^* + 1 + N_{S1}) + (G_1 - 1) \sqrt{\tau \eta} C_{p1}^* + G_1 \sqrt{\tau \eta} C_{p1} \right] + C_{p2}^* \sqrt{\tau \eta G_2 (G_1 - 1)}. \end{aligned} \quad (\text{B4})$$

Here  $N_S^* = \tau [N_{S1} \eta + N_{S2} (1 - \eta)] + N_B$ . The depen-

dence on the phases  $\theta_1, \theta_2$  lies in the phase-sensitive cor-

relations  $C_{p1}, C_{p2}$ .

Given  $V$ , we immediately have the covariance matrix of the quadratures  $\hat{q}'_{A'_k} = \hat{a}'_{A'_k} + \hat{a}'_{A'_k}^\dagger$ ,  $\hat{p}'_{A'_k} = -i(\hat{a}'_{A'_k} - \hat{a}'_{A'_k}^\dagger)$  for the two modes  $k = 1, 2$

$$V_{\text{quad}} \equiv \left\langle \begin{pmatrix} \hat{q}_1 \\ \hat{p}_1 \\ \hat{q}_2 \\ \hat{p}_2 \end{pmatrix} \begin{pmatrix} \hat{q}_1 & \hat{p}_1 & \hat{q}_2 & \hat{p}_2 \end{pmatrix} \right\rangle = \begin{pmatrix} E & 0 & C & 0 \\ 0 & E & 0 & C \\ C & 0 & S & 0 \\ 0 & C & 0 & S \end{pmatrix}, \quad (\text{B5})$$

which can be obtained via the relationship  $V_{\text{quad}} = UVU^\dagger$  with the transform matrix  $U$

$$U = \begin{pmatrix} 1 & 1 & 0 & 0 \\ -i & i & 0 & 0 \\ 0 & 0 & 1 & 1 \\ 0 & 0 & -i & i \end{pmatrix}. \quad (\text{B6})$$

The probability distribution of the random photon counts of such a two-mode Gaussian state with the quadrature covariance matrix Eq. (B5) is given by

$$P(n_1, n_2 | \theta_1, \theta_2) = -4F_R(1 + n_1, 1 + n_2, 1, \frac{4C^2}{XY}) \times \frac{(-1 + C^2 + E + S - ES)^{1+n_1+n_2}}{X^{1+n_1}Y^{1+n_2}}, \quad (\text{B7})$$

where  $F_R$  is the regularized hypergeometric function and  $X = 1 + C^2 + E - (1 + E)S$ ,  $Y = C^2 - (E - 1)(S + 1)$ . The information rates are then obtained via Eq. (21).

## 2. Serial PCR (Fig. 6b)

For the first OPA with a gain  $G_1$ ,

$$\begin{aligned} \hat{a}'_{B1} &= \sqrt{G_1} \hat{a}_B + \sqrt{G_1 - 1} \hat{a}_{v1}^\dagger, \\ \hat{a}'_{C1} &= \sqrt{G_1} \hat{a}_{v1} + \sqrt{G_1 - 1} \hat{a}_B^\dagger, \end{aligned} \quad (\text{B8})$$

where the ancilla  $\hat{a}_{v1}$  is in a vacuum mode. The following balanced beamsplitter yields two arms  $\hat{a}_{X1} = (\hat{a}'_{C1} + \hat{a}_{A'1})/\sqrt{2}$ ,  $\hat{a}_{Y1} = (\hat{a}'_{C1} - \hat{a}_{A'1})/\sqrt{2}$ . We measure the photon count differences of  $N_R$  i.i.d. copies between  $\hat{a}_{X1}$  and  $\hat{a}_{Y1}$ .

For the second OPA with a gain  $G_2$ ,

$$\begin{aligned} \hat{a}'_{B2} &= \sqrt{G_2} \hat{a}'_{B1} + \sqrt{G_2 - 1} \hat{a}_{v2}^\dagger, \\ \hat{a}'_{C2} &= \sqrt{G_2} \hat{a}_{v2} + \sqrt{G_2 - 1} \hat{a}'_{B1}^\dagger. \end{aligned} \quad (\text{B9})$$

Similarly the following balanced beamsplitter yields two arms  $\hat{a}_{X2} = (\hat{a}'_{C2} + \hat{a}_{A'2})/\sqrt{2}$ ,  $\hat{a}_{Y2} = (\hat{a}'_{C2} - \hat{a}_{A'2})/\sqrt{2}$ . We measure the photon count differences between  $\hat{a}_{X2}$  and  $\hat{a}_{Y2}$  of  $N_R$  i.i.d. copies. The modes  $\hat{a}_{X1}, \hat{a}_{Y1}, \hat{a}_{X2}, \hat{a}_{Y2}$  are in a zero-mean Gaussian state with the covariance matrix

$$V \equiv \left\langle \begin{pmatrix} \hat{a}'_{X1} \\ \hat{a}'_{Y1} \\ \hat{a}'_{X2} \\ \hat{a}'_{Y2} \end{pmatrix} \begin{pmatrix} \hat{a}'_{X1} & \hat{a}'_{Y1} & \hat{a}'_{X2} & \hat{a}'_{Y2} \end{pmatrix} \right\rangle = \begin{pmatrix} a_1 + 1 & 0 & c_1 & 0 & a_3 & 0 & c_{31} & 0 \\ 0 & a_1 & 0 & c_1^* & 0 & a_3^* & 0 & c_{31}^* \\ c_1^* & 0 & s_1 + 1 & 0 & c_{32} & 0 & s_3 & 0 \\ 0 & c_1 & 0 & s_1 & 0 & c_{32}^* & 0 & s_3^* \\ a_3^* & 0 & c_{32}^* & 0 & a_2 + 1 & 0 & c_2 & 0 \\ 0 & a_3 & 0 & c_{32} & 0 & a_2 & 0 & c_2^* \\ c_{31}^* & 0 & s_3^* & 0 & c_2^* & 0 & s_2 + 1 & 0 \\ 0 & c_{31} & 0 & s_3 & 0 & c_2 & 0 & s_2 \end{pmatrix}, \quad (\text{B10})$$

where the constants

$$\begin{aligned}
a_1 &= \frac{1}{2} \left( 2 \operatorname{Re}(C_{p1}) \sqrt{\eta(G_1 - 1)\tau} + \eta G_1 \tau N_{S1} - (\eta - 1)(G_1 - 1) \tau N_{S2} - \eta \tau N_{S1} + (G_1 - 1)(N_B + 1) + N_{S1} \right), \\
s_1 &= \frac{1}{2} \left( -2 \operatorname{Re}(C_{p1}) \sqrt{\eta(G_1 - 1)\tau} + \eta(G_1 - 1) \tau N_{S1} - (\eta - 1)(G_1 - 1) \tau N_{S2} + (G_1 - 1)(N_B + 1) + N_{S1} \right), \\
c_1 &= \frac{1}{2} \left( -2i \operatorname{Im}(C_{p1}) \sqrt{\eta(G_1 - 1)\tau} + \eta(1 - G_1) \tau N_{S1} + (\eta - 1)(G_1 - 1) \tau N_{S2} + (1 - G_1)(N_B + 1) + N_{S1} \right), \\
a_3 &= \frac{1}{2} \left( C_{p2}^* \sqrt{(1 - \eta)(G_1 - 1)\tau} + C_{p1} \sqrt{\eta G_1 (G_2 - 1)\tau} + \sqrt{(G_1 - 1)G_1 (G_2 - 1)} (N_S^* + 1) \right), \\
s_3 &= \frac{1}{2} \left( -C_{p2}^* \sqrt{(1 - \eta)(G_1 - 1)\tau} + C_{p1} \left( -\sqrt{\eta G_1 (G_2 - 1)\tau} \right) + \sqrt{(G_1 - 1)G_1 (G_2 - 1)} (N_S^* + 1) \right), \\
c_{31} &= \frac{1}{2} \left( C_{p2}^* \sqrt{(1 - \eta)(G_1 - 1)\tau} + C_{p1} \left( -\sqrt{\eta G_1 (G_2 - 1)\tau} \right) - \sqrt{(G_1 - 1)G_1 (G_2 - 1)} (N_S^* + 1) \right), \\
c_{32} &= \frac{1}{2} \left( -C_{p2}^* \sqrt{(1 - \eta)(G_1 - 1)\tau} + C_{p1} \sqrt{\eta G_1 (G_2 - 1)\tau} - \sqrt{(G_1 - 1)G_1 (G_2 - 1)} (N_S^* + 1) \right), \\
a_2 &= \frac{1}{2} \left( 2 \operatorname{Re}(C_{p2}) \sqrt{(1 - \eta)G_1 (G_2 - 1)\tau} + G_1 (G_2 - 1) (N_S^* + 1) + N_{S2} \right), \\
s_2 &= \frac{1}{2} \left( -2 \operatorname{Re}(C_{p2}) \sqrt{(1 - \eta)G_1 (G_2 - 1)\tau} + G_1 (G_2 - 1) (N_S^* + 1) + N_{S2} \right), \\
c_2 &= \frac{1}{2} \left( -2i \operatorname{Im}(C_{p2}) \sqrt{(1 - \eta)G_1 (G_2 - 1)\tau} - G_1 (G_2 - 1) (N_S^* + 1) + N_{S2} \right).
\end{aligned} \tag{B11}$$

The dependence on phase modulation  $\theta_1, \theta_2$  lies in the phase-sensitive correlations  $C_{p1}, C_{p2}$ .

As it is challenging to numerically evaluate the photon count distribution of a four-mode Gaussian state, we estimate the performance of PCRs by a Gaussian approximation. From the covariance matrix  $V$  of  $\hat{a}_{X1}, \hat{a}_{Y1}, \hat{a}_{X2}, \hat{a}_{Y2}$ , by Wick's theorem we immediately have the  $2 \times 2$  covariance matrix  $V_d$  of the photon differences  $\Delta \hat{N}_i = \hat{N}_{X_i} - \hat{N}_{Y_i} = \langle \hat{a}_{X_i} \hat{a}_{X_i} \rangle - \langle \hat{a}_{Y_i} \hat{a}_{Y_i} \rangle$  for the two slices  $i = 1, 2$ . Due to the central limit theorem, the mean distribution of  $N_R$  i.i.d. copies of random variables  $\Delta N_1, \Delta N_2$  converges to the Gaussian distribution when  $N_R \rightarrow \infty$

$$P(\mathbf{n}|\theta_1, \theta_2) = \frac{1}{(2\pi)^2 \sqrt{\det V_d^{(N_R)}}} \exp \left\{ -\frac{\mathbf{n}^T V_d^{(N_R)-1} \mathbf{n}}{2} \right\}, \tag{B12}$$

where  $V_d^{(N_R)} = V_d/M$  is the covariance matrix of the  $N_R$ -copy mean distribution,  $\mathbf{n}$  is the two-dimensional output

averaged over  $N_R$  copies of the random photon count differences  $\Delta N_1, \Delta N_2$ . The information rates are then obtained via Eq. (21).

### 3. Parallel OPAR (Fig. 6c)

At the receiver side we apply a beamsplitter to slice the returned mode  $\hat{a}_B$  into two copies  $i = 1, 2$

$$\hat{a}_{Bi} = \sqrt{\eta_i} \hat{a}_B + \sqrt{1 - \eta_i} \hat{a}_{vi}, \tag{B13}$$

where each ancilla  $\hat{a}_{vi}$  is in vacuum. For each OPA  $i = 1, 2$

$$\begin{aligned}
\hat{a}'_{Bi} &= \sqrt{G_i} \hat{a}_{Bi} + \sqrt{G_i - 1} \hat{a}_{A'i}^\dagger, \\
\hat{a}'_{A'i} &= \sqrt{G_i} \hat{a}_{A'i} + \sqrt{G_i - 1} \hat{a}_{Bi}^\dagger.
\end{aligned} \tag{B14}$$

We measure the photon counts of  $N_R$  i.i.d. copies of  $\hat{a}'_{A'1}, \hat{a}'_{A'2}$ . These modes are in a Gaussian state with the covariance matrix in the same form of Eq. (B3) valued by

$$\begin{aligned}
a &= \eta(G_1 - 1)N_B + 2\eta\sqrt{(G_1 - 1)G_1\tau} \operatorname{Re}(C_{p1}) + \eta(G_1 - 1)\tau(\eta N_{S1} + (1 - \eta)N_{S2}) + G_1 N_{S1} + G_1 - 1, \\
s &= (G_2 - 1) \left[ (1 - \eta)(N_B + \eta\tau N_{S1}) + (1 - \eta)^2\tau N_{S2} \right] + G_2(N_{S2} + 1) + 2(\eta - 1)\sqrt{(G_2 - 1)G_2\tau} \operatorname{Re}(C_{p2}) - 1, \\
c &= -\sqrt{(1 - \eta)\eta(G_2 - 1)} \left( \sqrt{G_1 - 1}N_S^* + C_{p1}\sqrt{G_1\tau} \right) + C_{p2}^* \sqrt{-(\eta - 1)\eta(G_1 - 1)G_2\tau}.
\end{aligned} \tag{B15}$$

where  $N_S^* = \tau[\eta N_{S1} + (1 - \eta)N_{S2}] + N_B$ . The photon

count distribution is given by Eq. (B7) with quadra-



ture covariance matrix evaluated by plugging  $a, s, c$  in Eq. (B5). The information rates are then obtained via Eq. (21).

#### 4. Parallel PCR (Fig. 6d)

By contrast with the parallel OPAR, at the receiver side we first apply the phase conjugation by an OPA to obtain

$$\hat{a}'_C = \sqrt{G}\hat{a}_v + \sqrt{G-1}\hat{a}_B^\dagger, \quad (\text{B16})$$

where the ancilla  $\hat{a}_v$  is in vacuum. Then a beamsplitter slices the mode  $\hat{a}'_C$  into two copies  $i = 1, 2$ ,

$$\hat{a}'_{Ci} = \sqrt{\eta_i}\hat{a}'_C + \sqrt{1-\eta_i}\hat{a}_{vi}. \quad (\text{B17})$$

For each slice  $i = 1, 2$ , a balanced beamsplitter yields two arms  $\hat{a}_{Xi} = (\hat{a}_{Ci} + \hat{a}_{A'i})/\sqrt{2}$ ,  $\hat{a}_{Yi} = (\hat{a}_{Ci} - \hat{a}_{A'i})/\sqrt{2}$ . We measure the photon count differences between  $\hat{a}_{Xi}$  and  $\hat{a}_{Yi}$  of  $N_R$  i.i.d. copies. Here  $\hat{a}_{X1}, \hat{a}_{Y1}, \hat{a}_{X2}, \hat{a}_{Y2}$  are in a zero-mean Gaussian state with the covariance matrix in the same form of (B10). The evaluation of parameters  $a_1, s_1, c_1, \dots$  is straightforward and lengthy, so we omit it here. A Gaussian approximation for the probability distribution of the measurement results follows from Eq. (B12). The information rates are then obtained via Eq. (21).

#### Appendix C: MAC HSW theorem

Consider the  $s$ -sender MAC  $\mathcal{M}$ . Here we deliberately use a different notation  $\mathcal{M}$  instead of  $\mathcal{N}$  for reasons that will become apparent later. The scenario of MAC classical communication without EA is similar to the EA case

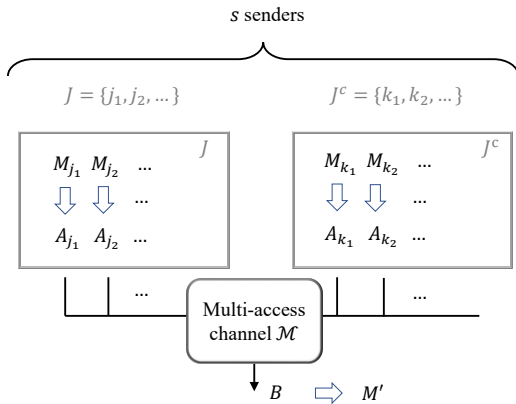


Figure 9. The protocol of general MAC communication. The  $s$  senders individually prepare the quantum states in the corresponding quantum system  $A_i$  given their messages in each codeword space  $M_i$ . The receiver reconstructs a message in codeword space  $M'$  decoded from the output in quantum system  $B$ .

in Fig. 1, except that the EA systems  $A'$  are gone. We also adopt the same notation, as shown in Fig. 9.

The receiver decodes the messages  $m = m_1 m_2 \dots m_s$  of all senders, of which the word space is denoted as  $M'$ . Accordingly, we can write the message as a bipartition  $m = m[J]m[J^c]$ . The input encoding of the MAC  $\{p_m, \hat{\sigma}_A^m\}$  involves sending each quantum state  $\hat{\sigma}_A^m$  through MAC  $\mathcal{M}$  by probability  $p_m$ . The overall state after the encoding is

$$\hat{\Xi}_{MA} = \sum_m p_m |m\rangle\langle m|_M \otimes \hat{\sigma}_A^m. \quad (\text{C1})$$

Note that due to the independence between the  $s$  senders, the overall probability and state of each encoding can be written as the products  $p_m = \prod_{i=1}^s p_{m_i}$ ,  $\hat{\sigma}_A^m = \otimes_{i=1}^s \hat{\sigma}_{A_i}^m$ , where  $A_i$  denote the quantum system of sender  $i$ . Alternatively, for an arbitrary bipartition  $J, J^c$ , we have  $p_m = p_{m[J]}p_{m[J^c]}$ ,  $\hat{\sigma}_A^m = \hat{\sigma}_{A[J]} \otimes \hat{\sigma}_{A[J^c]}$ . The MAC maps the composite input  $A$  to a single output quantum system  $B$ , leading to the output

$$\hat{\omega}_{MB} = \sum_m p_m |m\rangle\langle m|_M \otimes \mathcal{M}_{A \rightarrow B}(\hat{\sigma}_A^m). \quad (\text{C2})$$

With the above notations prepared, we can introduce the information theoretical quantities. To begin with, we introduce the conditional entropy

$$S(B|M[J^c])_{\hat{\omega}} = \sum_{m[J^c]} p_{m[J^c]} S\left[\mathcal{M}_{A \rightarrow B}\left(\sum_{m[J]} p_{m[J]} \hat{\sigma}_A^m\right)\right], \quad (\text{C3})$$

similarly, noting that  $M = M[J]M[J^c]$  and  $p_m = p_{m[J]}p_{m[J^c]}$  we can have the notation

$$S(B|M)_{\hat{\omega}} = \sum_m p_m S[\mathcal{M}_{A \rightarrow B}(\hat{\sigma}_A^m)]. \quad (\text{C4})$$

We introduce the conditional quantum mutual information

$$I(M[J]; B|M[J^c])_{\hat{\omega}} = S(B|M[J^c])_{\hat{\omega}} - S(B|M)_{\hat{\omega}} \quad (\text{C5})$$

With the notations introduced, we quote Theorem 10 of Ref. [36] to give the capacity region of MAC without EA, in preparation for the proof of Theorem 1.

**Theorem 2** For any  $s$ -sender MAC  $\mathcal{M}$  and encoding  $\{p_m, \hat{\sigma}_A^m\}$  associated with all senders'  $s$ -digit letter  $m$ , the rate region of reliable classical communication is given by a list of  $2^s$  inequalities,

$$\sum_{i \in J} R_i \leq I(M[J]; B|M[J^c])_{\hat{\omega}}, \quad (\text{C6})$$

for all bi-partition of  $J$  and  $J^c$  of the  $s$  users, where  $\hat{\omega}$  is defined in Eq. (C2) relying on the encoding.

In the EA protocol, the quantum system comes with a reference system  $A'$  which is pre-shared to the receiver

side intact, while the quantum system goes through the MAC  $\mathcal{N}$ . However, we can view the overall channel  $\mathcal{M} = \mathcal{N} \otimes \mathcal{I}$  as a single MAC. Note that the encoding is, however, restricted as the  $\mathcal{I}$  part corresponds to references.

#### Appendix D: Proof of Theorem 1

We derive the EA-MAC classical capacity in analogy to the single-sender single-receiver EA classical capacity [14] and the two-sender EA-MAC classical capacity [17].

Below we prove that both the inner and outer bounds of  $\mathcal{C}_E^{(1)}(\mathcal{N})$ . In the proof, we omit ‘ $\wedge$ ’ in the notation of operators for simplicity, since the meaning of each notation is clear in the context.

##### 1. Inner bound

We prove the inner bound by showing the boundaries achievable for any pure state  $\phi$ . We show that the  $2^s$  conditional quantum mutual information quantities in Eq. (C6) reach all the boundaries of  $\tilde{\mathcal{C}}_E$  region defined by Eq. (15). Then the achievability is proven, as Theorem 2 guarantees that a single POVM can achieve Eq. (C6) for all  $J$  simultaneously, which provides the inner bound. During the evaluation of entropies within this section,  $AA'$  is the relevant Hilbert space and we omit the sub-

scripts for states living in  $AA'$ .

We begin with the special case of each pair  $\{(A_i, A'_i), 1 \leq i \leq s\}$  being in a maximally entangled state, such that the reduced state  $\phi_{A_i} = \text{Tr}_{A' A_j \neq i}(\phi) = (I/d_i)_{A_i}$  is fully mixed, here the dimension  $d_i = \dim A_i$ . The capacity achieving protocol is implemented by a generator state being  $\phi$  and a correlation-removing unitary encoding  $\{U_m\}$ . In terms of the ensemble  $\sum_m p_m U_m \phi U_m^\dagger$ , a correlation-removing encoding  $\{U_m\}$  wipes out the correlation between each system  $A_i$  with its reference system. Concretely, this can be implemented by the generalized Pauli operators

$$U_{m_i} = T_{A_i}^{m_{i,T}} R_{A_i}^{m_{i,R}}, \text{ where} \quad (D1)$$

$$m_i = m_{i,T} m_{i,R}, 1 \leq m_{i,T} \leq d_i, 1 \leq m_{i,R} \leq d_i,$$

with the Pauli matrices  $T_{jk} = \delta_{j,k-1 \bmod d_i}$ ,  $R_{jk} = e^{i2\pi k/d_i} \delta_{jk}$  acting on each subspace  $A_i$ . Governed by the independence constraint of MAC,  $\phi = \otimes_{i=1}^s \phi_{A_i A'_i}$ . The encoding  $U_m = \otimes_{i=1}^s U_{m_i}$  acting on  $\otimes_{i=1}^s A_i$  by probability  $p_m = \prod_{i=1}^s p_{m_i}$  is also separable.

Now the overall quantum state after the channel is

$$\omega_{MBA'} = \sum_m p_m |m\rangle\langle m|_M \otimes [\mathcal{N}_{A \rightarrow B} \otimes \mathcal{I}] (U_m \phi U_m^\dagger). \quad (D2)$$

Applying Theorem 2 to Eq. (D2), we have an achievable information rate of this protocol

$$\begin{aligned} \sum_{i \in J} R_i &= I(M[J]; B | M[J^c])_\omega \\ &= \mathbb{E}_{m[J^c]} \left\{ S \left[ \mathcal{N} \otimes \mathcal{I} \left( \sum_{m[J]} U_{m[J]} U_{m[J^c]} \phi U_{m[J^c]}^\dagger U_{m[J]}^\dagger \right) \right] - \mathbb{E}_{m[J]} \left\{ S[\mathcal{N} \otimes \mathcal{I} (U_m \phi U_m^\dagger)] \right\} \right\}, \\ &= \mathbb{E}_{m[J^c]} \left\{ S \left[ \mathcal{N} \otimes \mathcal{I} \left( U_{m[J^c]} \phi_{A'[J^c]A} U_{m[J^c]}^\dagger \right) \right] + S(\phi_{A'[J]}) - \mathbb{E}_{m[J]} \left\{ S[\mathcal{N} \otimes \mathcal{I} (U_m \phi U_m^\dagger)] \right\} \right\}, \end{aligned} \quad (D3)$$

where  $\mathbb{E}_x[f(x)] \equiv \int dx p(x) f(x)$  refers to the expectation value of function  $f$  averaged on probability distribution  $p$ . The second equality is because  $\{U_{m[J]}\}$  is correlation-removing within system  $A[J]$ ,

$$\mathcal{N} \otimes \mathcal{I} \left( \sum_{m[J]} U_{m[J]} U_{m[J^c]} \phi U_{m[J^c]}^\dagger U_{m[J]}^\dagger \right) = \mathcal{N} \otimes \mathcal{I} \left( U_{m[J^c]} \phi_{A'[J^c]A} U_{m[J^c]}^\dagger \right) \otimes \phi_{A'[J]}. \quad (D4)$$

In contrast to the single-user case, here we see that the encoding restricted on  $A[J]$  fails to remove the correlation between  $A$  and  $A'[J^c]$ , so  $A'[J^c]$  is left with  $A$  in the entropy quantities.

Next, we note that for the maximally entangled state  $\phi$ , we have  $U \otimes I |\phi\rangle = I \otimes U^* |\phi\rangle$  for any unitary  $U$ . This equivalence ensures that the encoding preserves the

entropy of the output state

$$\begin{aligned} &S \left[ \mathcal{N} \otimes \mathcal{I} \left( U_{m[J^c]} \phi_{A'[J^c]A} U_{m[J^c]}^\dagger \right) \right] \\ &= S[\mathcal{N} \otimes \mathcal{I} (\phi_{A'[J^c]A})], \end{aligned} \quad (D5)$$

similarly

$$S[\mathcal{N} \otimes \mathcal{I} (U_m \phi U_m^\dagger)] = S[\mathcal{N} \otimes \mathcal{I} (\phi)]. \quad (D6)$$

Therefore, the averaging in  $\mathbb{E}_{m[J]}, \mathbb{E}_{m[J^c]}$  disappears in Eq. (D3). Therefore, Eq. (D3) reduces to

$$\sum_{i \in J} R_i = S(\mathcal{N} \otimes \mathcal{I}(\phi_{A'[J^c]A})) + S(\phi_{A'[J]}) - S(\mathcal{N} \otimes \mathcal{I}(\phi)). \quad (\text{D7})$$

Simplifying the right-hand-side above, we obtain

$$\begin{aligned} \sum_{i \in J} R_i &= S(BA'[J^c])_\rho + S(A'[J])_\rho - S(A'[J]BA'[J^c])_\rho \\ &= I(A'[J]; BA'[J^c])_\rho = I(A'[J]; B|A'[J^c])_\rho. \end{aligned} \quad (\text{D8})$$

Here we utilized the channel mapping  $\rho_{BA'} = \mathcal{N}_{A \rightarrow B} \otimes \mathcal{I}(\phi_{AA'})$ . And the last step is due to independence between the signals. Note that Eq. (D8) holds for any  $J$ . Hence Eq. (D3) achieves  $\tilde{\mathcal{C}}_E(\mathcal{N}, \phi)$  in Eq. (15) for the maximally entangled state.

Indeed, the achievability also holds for any *projection-like*  $\phi_A$ , which is proportional to a projection operator to some subspace  $\mathcal{S}$  of the input Hilbert space  $\mathcal{H}_{in}$ , along with the encoding  $\{U_{m[J]}\}$  restricted on  $\mathcal{S}$ . For now, we have achieved the rate region specified by Eq. (15) for all projection-like inputs.

Having proven the result for the special case of inputs with a projection-like reduced density matrix, now we extend the proof to general pure product states  $\phi$ . For simplicity here we denote the reduced density matrix as  $\xi \equiv \phi_A$ . First we introduce the  $n$ -letter  $\epsilon$ -typical space  $T_n(\xi)$  of an arbitrary single-letter state  $\xi = \sum_x p(x) |x\rangle\langle x|$ , where  $\{|x_i\rangle\}$  is an orthogonal set.  $T_n(\xi)$  comprises every typical states  $|x_1 x_2 \dots x_n\rangle$  associated with typical sequences  $x_1 x_2 \dots x_n$  satisfying

$$\left| -\log \left( \prod_{i=1}^n p(x_i) \right) / n - S(\xi) \right| \leq \epsilon. \quad (\text{D9})$$

Denote by  $P_{T_n}$  the projection operator onto subspace  $T_n(\xi)$ . The typicality follows from the law of large number, explicitly, for any  $\epsilon > 0$  there exists  $n$  sufficiently large such that the typical subspace almost includes the  $n$ -letter random encoding  $\xi^{\otimes n}$

$$\text{Tr} [\xi^{\otimes n} (I - P_{T_n})] \leq \delta. \quad (\text{D10})$$

Now let  $\pi_{T_n}$  be the normalized projection operator  $P_{T_n} / \dim T_n$ . By the definition of  $\epsilon$ -typicality Eq. (D9), the entropy of the uniform distribution  $\pi_{T_n}$  is almost  $nS(\xi)$  up to a prefactor  $\sim 1 - \delta$ , explicitly

$$(1 - \delta)2^{n(S(\xi) - \epsilon)} \leq \dim T_n(\xi) \leq 2^{n(S(\xi) + \epsilon)}. \quad (\text{D11})$$

By a similar correlation-removing encoding on  $\xi$ , below we show that the  $n$ -letter  $I(A'[J]; B|A'[J^c])_{\mathcal{N}^{\otimes n} \otimes \mathcal{I}(\pi_{T_n})}$  quantity achieves  $I(A'[J]; B|A'[J^c])_{\mathcal{N} \otimes \mathcal{I}(\xi)}$ .

The typicality Eq. (D11) gives the first term in Eq. (D7). Meanwhile, for the last two terms in Eq. (D7), we construct a unitary  $\mathcal{U}$  including the environment mode

to simulate channel  $\mathcal{N}$ . Denote the complementary channel as  $\mathcal{K}$ , which maps the input state to the environment mode. Define  $\Phi_{\pi_{T_n}}$  as a purification of  $\pi_{T_n}$  fulfilled per system pair  $A_i A'_i$ ,  $1 \leq i \leq s$ . Then the last term  $S[(\mathcal{N} \otimes \mathcal{I})^{\otimes n} \Phi_{\pi_{T_n}}] = S[\mathcal{K}(\pi_{T_n})]$ , thereby the latter two terms converges to the desired quantity when  $\epsilon \rightarrow 0$

$$\begin{aligned} S[\mathcal{N}^{\otimes n}(\pi_{T_n})] - S[\mathcal{K}(\pi_{T_n})] \\ \rightarrow n[S(\mathcal{N} \otimes \mathcal{I}(\xi)) - S(\mathcal{N} \otimes \mathcal{I}(\Phi_\xi))] , \end{aligned} \quad (\text{D12})$$

which follows from Lemma 1 in [14]. Following a similar procedure to the proof for maximally entangled state, both sides of the equation above can be reduced to a conditional quantum information quantity:  $I(A'[J]; B|A'[J^c])_\rho$  with  $\rho = \mathcal{N}^{\otimes n} \otimes \mathcal{I}(\Phi_{\pi_{T_n}})$  for LHS, and  $nI(A'[J]; B|A'[J^c])_\rho$  with  $\rho = \mathcal{N} \otimes \mathcal{I}(\phi)$  for RHS. Combining the above together, we have the information rate per letter

$$\begin{aligned} I(A'[J]; B|A'[J^c])_{\mathcal{N}^{\otimes n} \otimes \mathcal{I}(\Phi_{\pi_{T_n}})} / n \\ \rightarrow I(A'[J]; B|A'[J^c])_{\mathcal{N} \otimes \mathcal{I}(\phi)} \end{aligned} \quad (\text{D13})$$

given  $\epsilon \rightarrow 0$ . Note that  $\pi_{T_n}$  is projection-like thus  $I(A'[J]; B|A'[J^c])_{\mathcal{N}^{\otimes n} \otimes \mathcal{I}(\Phi_{\pi_{T_n}})}$  is achievable. Hence,  $I(A'[J]; B|A'[J^c])_{\mathcal{N} \otimes \mathcal{I}(\phi)}$  is achievable for any pure product state  $\phi$ .

Now we have proven  $\tilde{\mathcal{C}}_E$  specified by Eq. (15) is achievable for any input  $\phi$ . Then the one-shot capacity region is inner bounded by the union of  $\tilde{\mathcal{C}}_E(\mathcal{N}, \phi)$  regions over all possible  $\phi$

$$\mathcal{C}_E^{(1)}(\mathcal{N}) \supseteq \bigcup_{\phi} \tilde{\mathcal{C}}_E(\mathcal{N}, \phi). \quad (\text{D14})$$

## 2. Outer bound

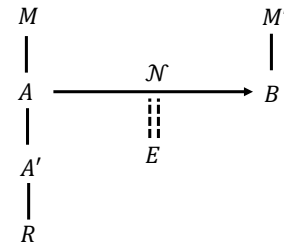


Figure 10. For the proof of the outer bound,  $A, B$  are the input and output systems of our MAC  $\mathcal{N}$ ,  $M, M'$  are the input and output code spaces.  $A'$  is the entanglement assistance system. System  $R$  purifies system  $A$  per subsystem  $A_i$ ,  $1 \leq i \leq s$ .

To prove the outer bound, we begin with the single-letter case. According to Theorem 2, given the encoding  $\{p_m, \sigma^m\}$ , the information rates  $\sum_{i \in J} R_i$  are upper bounded by

$$\sum_{i \in J} R_i \leq I(M[J]; BA'|M[J^c])_\omega. \quad (\text{D15})$$

where the state  $\omega$  is defined in Eq. (3). To ease the proof, we introduce reference systems  $R, E$ , as shown in Fig. 10.  $R = \otimes_{i=1}^s R_i$  individually purifies per sender  $i$  the subsystem  $\Xi_{M_i A_i A'_i}$  of the overall state  $\Xi_{MAA'}$  just after encoding, defined by Eq. (2). The environment system  $E$  purifies the overall state, including the system  $R$ , just after the channel. The channel is extended to a unitary transform  $\mathcal{U}_N : AE \rightarrow BE$  when  $E$  is included. We denote the purification before channel as  $\xi = \xi_{MAA'RE}$ , and the final purification after channel as  $\eta = \eta_{MBA'RE} = \mathcal{U}_N(\xi)$ . Below we show that  $I(M[J]; BA'|M[J^c])_\omega$  is upper bounded by the right-hand side of Eq. (15).

Equivalently, since the purification systems  $R, E$  are traced out at the end and make no difference, we evaluate  $I(M[J]; BA'|M[J^c])_\omega$  over  $\eta$

$$\begin{aligned} I(M[J]; BA'|M[J^c])_\eta &= I(M[J]; BA'M[J^c])_\eta \\ &= I(M[J]A'[J]; BA'[J^c]M[J^c])_\eta \\ &\quad - I(A'[J]; BA'[J^c]M[J^c])_\eta + I(M[J]; A'[J])_\eta. \end{aligned} \quad (\text{D16})$$

The first equality is due to the independent constraint of MAC  $I(M[J^c]; M[J]) = 0$ . The second equality is due to the chain rule of quantum mutual information. Let  $M[J] = X$ ,  $BA'[J^c]M[J^c] = Y$  and  $A'[J] = Z$ , we have  $I(M[J]; BA'M[J^c])_\eta = I(X; YZ) = I(Y; X|Z) + I(X; Z) = I(XZ; Y) - I(Z; Y) + I(X; Z)$ , which equals the second line term by term. Note that the encoding does not affect the entanglement assistance  $A'$ , thus

$$I(M[J]; A'[J])_\eta = 0, \quad (\text{D17})$$

and from the positivity of quantum mutual information

$$I(A'[J]; BA'[J^c]M[J^c])_\eta \geq 0, \quad (\text{D18})$$

we have

$$I(M[J]; BA'|M[J^c])_\eta \leq I(M[J]A'[J]; BA'[J^c]M[J^c])_\eta. \quad (\text{D19})$$

As EA is unlimited, there is always an expanded system  $A'_{ex} = \otimes_{i=1}^s A'_{ex,i}$  available that includes  $A'_i, R_i, M_i$  for each sender  $i$ . Adopting the expanded EA,

$$I(M[J]A'[J]; BA'[J^c]M[J^c])_\eta \leq I(A'_{ex}[J]; BA'_{ex}[J^c])_\eta, \quad (\text{D20})$$

since discarding systems never increases quantum information. Note that  $I(A'_{ex}[J^c]; A'_{ex}[J]) = 0$ , combining Ineqs. (D15) and (D19) and the above, we obtain the outer bound

$$\sum_{i \in J} R_i \leq I(B; A'_{ex}[J]|A'_{ex}[J^c])_\eta \quad (\text{D21})$$

for some pure state  $\eta$ , which is a product between different senders. Note that the state  $\eta$  and the channel output  $\mathcal{U}_N$  of any purification  $\Phi_{\Xi_A}$  leads to the same value of  $I(M[J]; BA'|M[J^c])$  after the channel, as their input state  $\xi$ ,  $\Phi_{\Xi_A}$  are identical up to a unitary transform on the entanglement assistance  $A'_{ex}$ . With the expanded entanglement assistance  $A' \equiv A'_{ex}$ , we arrive at the desired outer bound for any encoding  $\Xi$

$$\sum_{i \in J} R_i \leq I(B; A'[J]|A'[J^c])_\rho, \quad (\text{D22})$$

evaluated on the channel output  $\rho = \mathcal{N} \otimes \mathcal{I}(\phi)$  of some pure product state  $\phi = \phi_{AA'}$  that purifies the reduced state  $\Xi_A$ .

Denote  $\{\mathcal{T}\}_\phi$  as a family of encodings, of which the overall state after the encoding satisfies  $\Phi_{\Xi_A} = \phi$ . Now we have the outer bounds of the rate region Eq. (D22) of  $\{\mathcal{T}\}_\phi$  for each  $J$ , which form the region  $\tilde{\mathcal{C}}_E(\mathcal{N}, \phi)$ . Iterating over all encoding sets  $\{\mathcal{T}\}$ , it forbids the rate vector  $(R_1, R_2, \dots, R_s)$  from the intersection of the complementary sets of  $\tilde{\mathcal{C}}_E(\mathcal{N}, \phi)$  region, denoted as  $cp[\tilde{\mathcal{C}}_E(\mathcal{N}, \phi)]$ . The union  $\bigcup_\phi \{\mathcal{T}\}_\phi$  over all possible  $\phi$  spans all possible encodings. Thus the capacity region is outer bounded by the intersection of all complementary sets  $cp[\tilde{\mathcal{C}}_E(\mathcal{N}, \phi)]$  over all possible  $\phi$

$$\mathcal{C}_E^{(1)}(\mathcal{N}) \subseteq cp \left\{ \bigcap_\phi cp[\tilde{\mathcal{C}}_E(\mathcal{N}, \phi)] \right\} = \bigcup_\phi \tilde{\mathcal{C}}_E(\mathcal{N}, \phi). \quad (\text{D23})$$

Note that  $\Phi_{\Xi_A}$  is always pure and a product state per system pair  $A_i A'_i$  for  $1 \leq i \leq s$ , this region is a subset of  $\bigcup_\phi \tilde{\mathcal{C}}_E(\mathcal{N}, \phi)$  defined by Eq. (15).